Electrical transport properties of single-crystal CaB_6, SrB_6, and BaB_6

Jolanta Stankiewicz,[1] Priscila F. S. Rosa,[2] Pedro Schlottmann,[3] and Zachary Fisk[4]
[1]*Departamento de Física de la Materia Condensada and Instituto de Ciencia de Materiales de Aragón, CSIC-Universidad de Zaragoza, 50009 Zaragoza, Spain*
[2]*Department of Physics and Astronomy, University of California, Irvine, California 92697, USA and Los Alamos National Laboratory, Los Alamos, New Mexico 87545, USA*
[3]*Department of Physics, Florida State University, Tallahassee, Florida 32306, USA*
[4]*Department of Physics and Astronomy, University of California, Irvine, California 92697, USA*
(Received 31 May 2016; revised manuscript received 2 September 2016; published 22 September 2016)

The electrical resistivity and Hall effect of alkaline-earth-metal hexaboride single crystals are measured as a function of temperature, hydrostatic pressure, and magnetic field. The transport properties vary weakly with the external parameters and are modeled in terms of intrinsic variable-valence defects. These defects can stay either in (1) delocalized shallow levels or in (2) localized levels resonant with the conduction band, which can be neutral or negatively charged. Satisfactory agreement is obtained for electronic transport properties in a broad temperature and pressure range, although fitting the magnetoresistance is less straightforward and a combination of various mechanisms is needed to explain the field and temperature dependences.

DOI: 10.1103/PhysRevB.94.125141

I. INTRODUCTION

Alkaline-earth-metal hexaborides have attracted researchers' interest for over two decades. This has been triggered by the discovery of an unusual type of ferromagnetism in CaB_6 [1] and SrB_6 [2]. Neither the extensive theoretical and experimental work that followed on the electronic properties of CaB_6 [3] nor the more recent defect structure calculations [4], experiments under pressure [5–7], and reports on structural and magnetic properties of nanocrystalline CaB_6 [8] have led to a significantly deeper understanding of these intricate phenomena.

The continuing interest in hexaborides with cations of the alkaline-earth-metal series (E_AB_6; E_A = Ca,Sr,Ba) stems also from the diverse behavior shown by this class of materials attributed to their native defects. The homogeneity range of the series is not easy to establish, and most likely slight deviations from stoichiometry lead to some of the discrepancies encountered in many reports on the properties of E_AB_6.

Divalent hexaborides have a simple cubic unit cell (a CsCl-type structure). Electronic-structure calculations predict a sizable gap between the valence and the conduction bands at the X point in the Brillouin zone [9–11]. This has been corroborated by angle-resolved photoemission spectroscopy experiments on CaB_6 and SrB_6 [12,13]. In addition, a small electronlike spheroidal Fermi surface, centered at the X point, is seen in some of these studies [13]. Such an observation is consistent with electrical transport properties which are usually found to be metallic, thus placing E_AB_6 at the boundary between semimetals and insulators. Experimental results show that the native defects are mainly donors, most likely brought about by cation vacancies or unintentional impurities [14–19]. Despite many reports, a clear picture for electronic transport in alkaline-earth-metal hexaborides is still lacking. Our aim is to establish a coherent pattern of electronic transport in these compounds.

The measured variation of the electrical resistivity and of the Hall effect with temperature, hydrostatic pressure, and magnetic field show the complexity of native donors in divalent hexaborides. Previously, we reported electrical resistivity and Hall-effect behavior in CaB_6 single crystals of different carrier concentrations. The temperature variation of these properties was accounted for by a model in which B-antisite defects (a Ca atom substituted by a B atom) were "amphoteric" [20]. Here, we report results on an electronic transport study of SrB_6 and BaB_6 in addition to CaB_6 single crystals. The electron concentration in these crystals spans three orders of magnitude, a much larger range than the one studied before. This allows us to draw new conclusions about the nature of the native defects and their role in the transport properties of alkaline-earth-metal hexaborides. In particular, we propose that these defects give rise to resonant levels within the conduction band. This idea was first introduced in solid-state physics for metals [21], but resonant levels occur in many semiconductors [22]. We have before suggested such an energy scheme for B-antisite defects in CaB_6, but the explanation we now report differs from the previous one.

We hypothesize that each native donor gives rise to two types of electronic states: a delocalized shallow level and a more localized level, resonant with the conduction band, possibly emerging through lattice relaxation. In our relatively highly doped samples, a donor ion may also capture two electrons giving rise to negatively charged localized centers. The energy of the resonant levels is found to depend on electron concentration through mutual exchange and Coulomb interactions. The Fermi level is effectively pinned to the neutral defect level at low temperatures. In addition, our results seem to show that the defect centers are not related to any single conduction-band minimum. This model accounts well for measured temperature and pressure variations of the electron concentrations in E_AB_6. However, the modeling of the magnetoresistance (MR) behavior becomes quite complex because of the variety of contributions and parameters it involves.

II. EXPERIMENT

The single crystals of E_AB_6 used in our study were grown from Al flux with no intentional doping. The crystals were

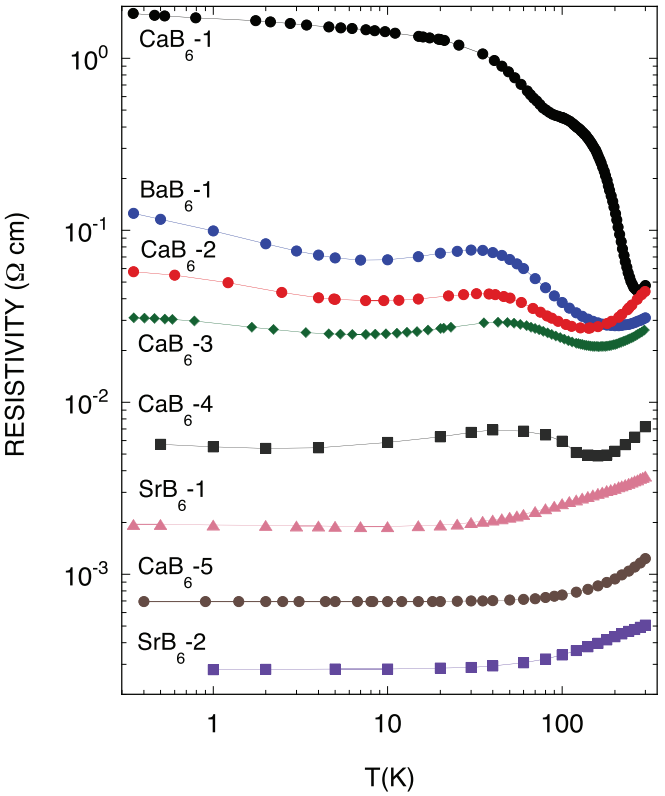

FIG. 1. Variation of electrical resistivity with temperature for E_AB_6 (E_A = Ca,Sr,Ba) single crystals.

shaped into either thin platelets or prisms. All measurements were performed on small single crystals of approximately $0.1 \times 0.5 \times 3$ mm^3. Prior to experiments, the crystals were cleaved and polished. We etched them in concentrated HCl acid before attaching contacts. Contact leads (25-μm gold wire) were spot welded to the samples. Low-frequency transport measurements were carried out in helium cryostats with a six- or four-probe method. The resistivity and Hall effect were measured as a function of the magnetic field of up to 10 T. Clamp cells with a liquid (Daphne oil 7373) as a pressure-transmitting medium [23] were used for measurements under pressures of up to 30 kbars in a Quantum Design physical property measurement system. We have found no large sample-to-sample variations of the electrical parameters in any growth batch of SrB_6 and BaB_6 crystals. For CaB_6, on the other hand, these parameters are more sample dependent.

III. RESULTS AND DISCUSSION

A. Temperature and pressure variation of resistivity and electron concentration

The variation of the electrical resistivity with temperature in stoichiometric E_AB_6 single crystals is shown in Fig. 1. The differences in conductivity of these crystals arises from the self-doping. We found that the electronic transport is very similar for all alkaline-earth-metal cations in the E_AB_6 compounds we have studied. Table I gives the values of electrical parameters at 2 and 295 K for the samples discussed in this paper.

TABLE I. Electrical transport parameters obtained for E_AB_6 (E_A = Ca,Sr,Ba) single crystals from resistivity and Hall-effect measurements.

Sample	n (2 K) (cm^{-3})	ρ (2 K) (Ω cm)	n (295 K) (cm^{-3})	ρ (295 K) (Ω cm)
CaB_6-1	5.56×10^{17}	1.6310	8.69×10^{17}	0.0478
BaB_6-1	6.12×10^{17}	0.0835	8.64×10^{17}	0.0305
CaB_6-2	9.45×10^{17}	0.0448	1.09×10^{18}	0.0442
CaB_6-3	1.65×10^{18}	0.0268	1.60×10^{18}	0.0263
CaB_6-4	9.01×10^{18}	0.0054	6.82×10^{18}	0.0071
SrB_6-1	2.01×10^{19}	0.00267	1.62×10^{19}	0.00515
CaB_6-5	3.65×10^{19}	0.00069	3.38×10^{19}	0.00123
SrB_6-2	1.14×10^{20}	0.00022	9.65×10^{19}	0.00040

Our measurements on different crystals show that the resistivity spans nearly five orders of magnitude. However, in each sample, the resistivity varies relatively little with temperature. As described in the previous report, upon lowering the temperature from 300 K, the resistivity $\rho(T)$ first decreases and subsequently increases in all but the more heavily doped crystals. $\rho(T)$ shows another broad minimum at approximately 10 K in lightly doped crystals and increases at lower temperatures. At the lowest temperatures, we find that the conductivity $\sigma \propto T^{1/2}$. This is shown in Fig. 2 for some E_AB_6 samples.

In Fig. 3 we plot the Hall resistivity ρ_H vs temperature. A broad maximum around 100 K is observed in $\rho_H(T)$ for lightly doped samples. This maximum moves to higher temperatures as self-doping becomes larger. We found electron-type conduction for all of our samples since ρ_H decreases linearly with the magnetic field (not shown), up to at least 5 T, in the temperature range we have studied. Figure 4 shows the dependence of the Hall coefficient R_H and the resistivity on the hydrostatic pressure p in some of the samples at two different

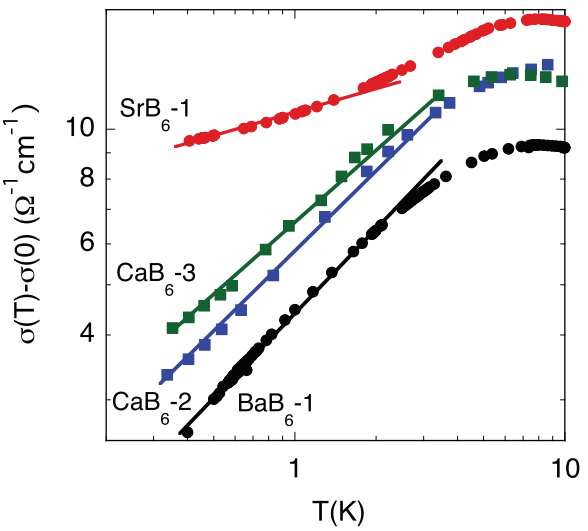

FIG. 2. The difference between the conductivity and its extrapolated zero-temperature value is plotted vs temperature for some of the E_AB_6 single crystals. Below approximately 5 K, the power-law dependence has exponent 1/2.

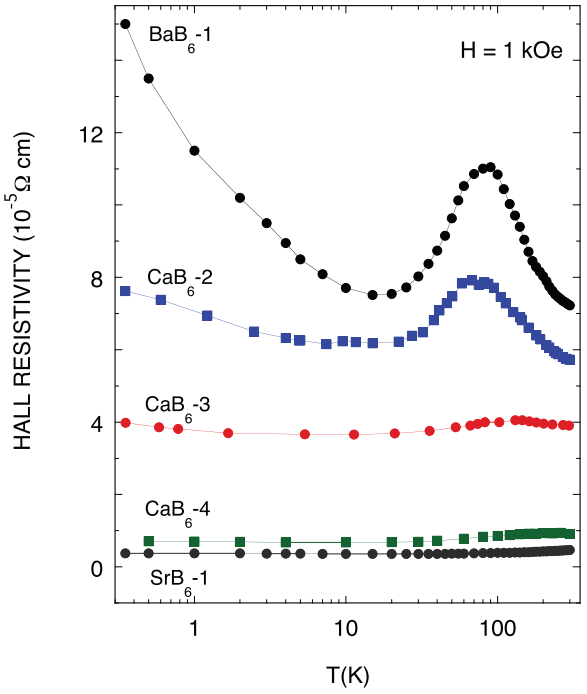

FIG. 3. Variation of Hall resistivity with temperature for E_AB_6 (E_A = Ca, Sr, Ba) single crystals.

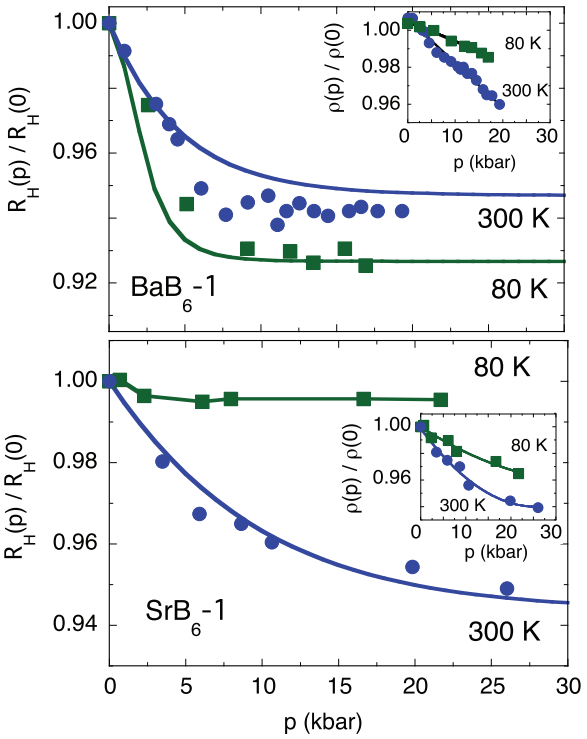

FIG. 4. Hall coefficient dependence on hydrostatic pressure for BaB_6 (upper panel) and SrB_6 (lower panel) single crystals at two different temperatures. The solid lines are fits to experimental data points using the variable-valence defects model. The insets show how the resistivity for the above crystals varies with pressure.

temperatures. In general, the experimental results obtained under pressure do not change significantly with temperature for temperatures less than 100 K. For the lightly doped BaB_6 single crystal, R_H drops initially with applied pressure and saturates beyond $p \approx 8$ kbars at both 80 and 300 K. For the SrB_6 sample with a much higher level of self-doping, R_H barely changes with p up to 25 kbars at $T = 80$ K. At higher temperatures, the Hall coefficient decreases with p. The results obtained for the CaB_6-3 sample (not shown) are in line with this behavior.

The temperature variation of the Hall coefficient found in E_AB_6 single crystals is anomalous. The hump around or above 100 K cannot be accounted for by a simple impurity band contribution or other two-carrier models. To explain these results, we assume that the intrinsic defects form an impurity band which merges with the conduction band. Therefore, we have given positive charges to substitutional donors d^+ which are in extended states. These centers may bind electrons and give rise to neutral localized centers d^0 with energy E_1. In addition, negatively charged localized donor states d^- at the energy E_2 exist. In highly doped materials, these states may occur from the capture of two electrons by a donor ion according to the reaction: $d^+ + 2e \rightarrow d^-$ [24]. The number of d^+, d^0, and d^- states (n_+, n_0, and n_+, respectively) is obtained from the statistics of multicharged centers in semiconductors [25,26]. Accordingly,

$$n_+ = \frac{N_{def}}{1 + \frac{g_0}{g_+} e^{(\eta-\varepsilon_1)} + \frac{g_-}{g_+} e^{(2\eta-\varepsilon_2)}}, \tag{1}$$

$$n_0 = \frac{N_{def} \frac{g_0}{g_+} e^{\eta-\varepsilon_1}}{1 + \frac{g_0}{g_+} e^{(\eta-\varepsilon_1)} + \frac{g_-}{g_+} e^{(2\eta-\varepsilon_2)}}, \tag{2}$$

$$n_- = \frac{N_{def} \frac{g_-}{g_+} e^{2\eta-\varepsilon_2}}{1 + \frac{g_0}{g_+} e^{(\eta-\varepsilon_1)} + \frac{g_-}{g_+} e^{(2\eta-\varepsilon_2)}}, \tag{3}$$

where N_{def} is the total concentration of the native defects; $g_i = g_i' e^{S_i/k_B}$, g_i' is the set of statistical weights for states $i = +$, 0, and $-$, corresponding to the donor ion with no electron, with one electron, and with two electrons, respectively, and S_i is the vibrational entropy of these states; $\varepsilon_1 = E_1/k_BT$ and $\varepsilon_2 = E_2/k_BT$ are the reduced energies of one and two electrons, respectively, $\eta = E_F/k_BT$, E_F is the energy of the Fermi level with respect to the bottom of the conduction band, and k_B is Boltzmann's constant. The electron concentration $n_{el}(T)$ in the conduction band satisfies the neutrality condition,

$$n_{el} = N_I + n_+ - n_-, \tag{4}$$

where $N_I = N_D - N_A$, N_A, and N_D are the concentrations of additional acceptor and donor impurities in the crystals, respectively. Here, we assume the hole concentration in the valence band is negligible. The statistical weights for the three charge states of the defect are $g_i' = 1$, 2, and 1 ($i = +$, 0, and $-$), respectively, if only the spin degeneracy is taken into account. The vibrational and configurational entropy content is more difficult to estimate. Although the contribution of localized impurities to the free-electron energy is negligible in most cases [27], we find that our fits improve assuming a small ($\approx 3 \times 10^{-4}$ eV/K for the E_1 state and 10^{-5} eV/K for the E_2 state) entropy content [17].

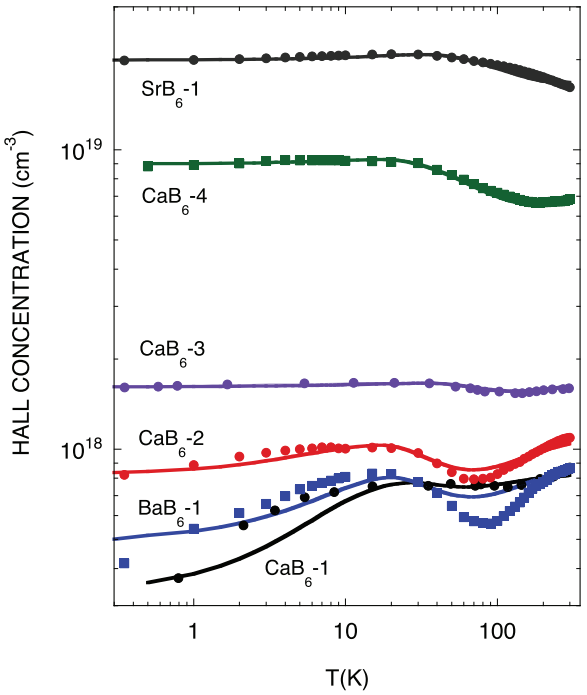

FIG. 5. Hall electron concentration vs temperature for various E_AB$_6$ single-crystal samples. The solid lines are fits to experimental data points using the variable-valence defects model.

Figure 5 shows the variable-valence defects model fits of the measured temperature variation of the electron concentration ($n_{el} = 1/eR_H$) in various E_AB$_6$ single crystals. Our fitting parameters are as follows: E_1, E_2, N_{def}, and N_I. The n_{el} is calculated by numerical integration of the standard density-of-state expression for a parabolic band with effective masses of $0.28m_o$ for CaB$_6$ [10], $0.22m_o$ for BaB$_6$ [9], and $0.27m_o$ for SrB$_6$ [28]. Here, m_o is the free-electron mass. The experimental behavior of the electron concentration, both for lightly and for more heavily doped crystals, is reproduced rather well by our model. The Fermi level is effectively pinned to the E_1 defect level at low temperatures. In Fig. 6 we plot the energies E_1 and E_2 as a function of the electron concentration in the conduction band. Since E_2 is the energy of the two-electron state, $E_2 > 2E_1$ at $T = 0$ is expected because of the electron-electron repulsion. The parameter $U_{eff} = E_2 - 2E_1$ is also plotted in Fig. 6. It only depends weakly on n_{el} even though both E_1 and E_2 vary with n_{el} noticeably. This variation arises mainly from the mutual exchange and Coulomb interactions between the electrons which show up as an effective increase in the energy of the defects [29,30]. The Coulomb interactions among the electrons themselves lead to the lowering of the energy of the conduction band by approximately [29],

$$\Delta E = -\frac{2e^2 k_F}{\pi\epsilon}\left[1 + \frac{\pi\lambda}{2k_F} - \frac{\lambda}{k_F}\tan^{-1}\left(\frac{k_F}{\lambda}\right)\right], \qquad (5)$$

where $k_F = (3\pi^2 n/\nu)^{1/3}$ is the Fermi wave vector (ν is the number of the conduction-band minima), ϵ is the dielectric constant ($\epsilon \approx 6$) [28], and $\lambda = (6\pi n_{el} e^2/\epsilon E_F)^{1/2}$ is the Thomas-Fermi screening parameter. The downward shift of the conduction band is further enhanced by the attractive

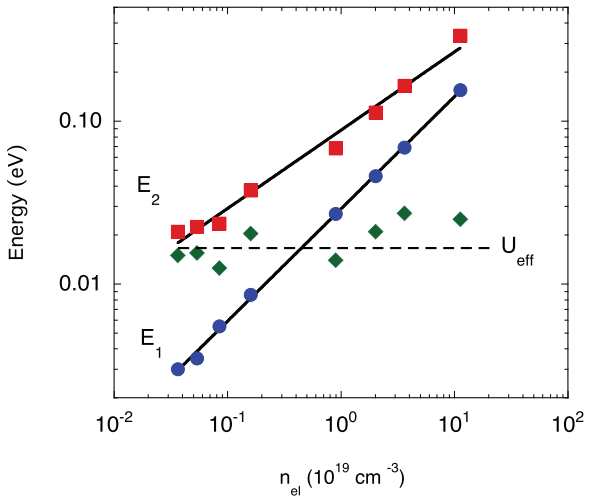

FIG. 6. Fitting parameters E_1 (circles) and E_2 (squares) vs electron concentration in E_AB$_6$ single crystals. $U_{eff} = E_2 - 2E_1$ is the energy of on-site repulsion (rhombus). The solid and dotted lines are to guide the eye.

interaction between the conduction carriers and the ionized d^+ donors whose magnitude has been estimated as $\Delta E \approx -4\pi n_{el} e^2/\epsilon a_B \lambda^3$, where e is the electron charge and a_B is the Bohr radius. In addition, the Coulomb interaction between negatively charged defect centers and conduction electrons may raise the defects' energies. All these corrections give a total of about 30 meV for $n_{el} = 1 \times 10^{19}$ cm^{-3}, which agrees with our data. We note that E_2 in Fig. 6 closely follows a $n^{1/2}$ dependence pointing to the importance of conduction electron-impurity scattering. The values of E_1, E_2, N_{def}, and N_I are listed in Table II.

The fit to the Hall data could be improved by taking into account the many-valley nature of the conduction band in E_AB$_6$ in the same way as has been performed to explain the electrical transport anomalies of Sb-doped Ge [31]. The maxima in the resistivity and Hall coefficient, observed at $T \approx T_F$ (T_F is the Fermi temperature), have been attributed to strong electron scattering when the temperature-dependent Thomas-Fermi screening parameter (k_{TF}) becomes comparable to

TABLE II. Energies of one- (E_1) and two-electron (E_2) levels, concentration of the native defects N_{def}, and concentration of additional impurities N_I obtained from the fit of our model to the temperature variation of the electron concentration in E_AB$_6$ (E_A = Ca,Sr,Ba) single crystals.

Sample	E_1 (eV)	E_2 (eV)	N_{def} (cm^{-3})	N_I (cm^{-3})
CaB$_6$-1	0.0030	0.018	7.3×10^{17}	1.0×10^{17}
BaB$_6$-1	0.0035	0.019	9×10^{17}	0
CaB$_6$-2	0.0055	0.018	1.1×10^{18}	0
CaB$_6$-3	0.0086	0.029	1.5×10^{18}	2.0×10^{18}
CaB$_6$-4	0.027	0.040	7.2×10^{18}	2.5×10^{18}
SrB$_6$-1	0.046	0.067	2.1×10^{19}	1.0×10^{18}
CaB$_6$-5	0.068	0.096	3.2×10^{19}	5.5×10^{18}
SrB$_6$-2	0.155	0.180	8.3×10^{19}	2.95×10^{19}

the Fermi wave vector in this many-valley semiconductor [32]. For single-valley cases, the range of the scattering potential is always larger than the Fermi wavelength, and such enhancement of scattering does not happen. Pertinent calculation involves various approximations in order to take into account nonlinear screening, many-body effects, and multiple scattering. In addition, it requires the knowledge of many band parameters which, at present, are not well established for E_AB_6 compounds. All of these prevented us from performing this task.

Further support for our variable-charge defect model comes from experiments under hydrostatic pressure. The observed drop of R_H vs p (see Fig. 4) can only be brought about by the rise in energy of the defect levels with respect to the minimum of the conduction band and, consequently, their depopulation. The solid lines in Fig. 4 show the calculated variation of the Hall coefficient R_H with p using the parameters deduced above and a value of 3 meV/kbars for dE_1/dp and dE_2/dp. We assume $dE_1/dp = dE_2/dp$ since nearly the same values of these coefficients have been found for other compounds [33]. The model fits the experimental data very well for all the compounds we have studied. The increase in the energy of the defects could be attributed to the downward pressure shift of the X-point conduction minimum as had been suggested for EuB_6 [34]. However, such conjecture disagrees with the experimental observation that the interband energy gaps increase with pressure [35]. Furthermore, recent high-pressure synchrotron x-ray-diffraction studies of BaB_6 show a decrease in the lattice constant pointing to an increase with pressure of the energy gap in this compound [36]. Therefore, some other mechanism should lie behind this effect. In addition, our results seem to show that the localized defect centers are not related to any single conduction-band minimum since its variation with pressure differs considerably from the shifts of the Γ or X points. We find that neither the energy nor the pressure coefficient of the localized defect centers vary significantly with temperature.

The question arises if the localized levels we infer from electrical transport measurements are coupled to the lattice and, therefore, metastable [33,37]. To this end we performed Hall-effect and resistivity measurements illuminating the CaB_6-3 sample at low temperatures with an IR LED, operating at a wavelength of about 910 nm. A small (about 2%) increase has been observed in R_H only when the illumination was on and for $T < 30$ K. Under these conditions, the resistivity becomes larger by approximately the same amount. Interestingly, a very weak negative magnetoresistance below approximately 2 kOe appears. None of these effects is persistent. Thus, we conclude that defect-lattice coupling is not important in E_AB_6.

B. Temperature and pressure variation of mobility

Figure 7 shows the temperature dependence of the low-field Hall mobility, obtained from $\mu_H = R_H/\rho$. For crystals with less than 10^{19} defects per cm^{-3}, the mobility first increases with decreasing temperature. Below approximately 150 K, it drops rapidly and goes through a shallow minimum to a nearly constant value at low temperatures. In the more resistive samples, μ_H drops (below 10 $cm^2\,V^{-1}\,s^{-1}$) to quite small values at low temperatures. In heavily doped crystals, the Hall

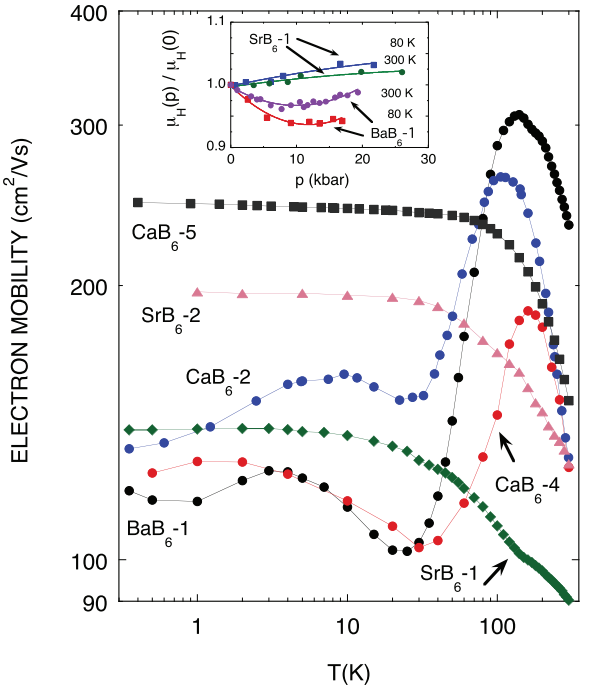

FIG. 7. Temperature variation of the Hall mobility for E_AB_6 single crystals. The inset shows how the mobility changes with pressure for two samples.

mobility is constant for $T \lesssim 80$ K and decreases at higher temperatures.

Carrier mobilities in a moderately doped semiconductor are usually limited by electron-phonon scattering and, at lower temperatures, by ionized impurity scattering. Close to room temperature, the mobility in our crystals varies as $T^{-3/2}$. From this, we infer that acoustic phonon scattering limits the mobility. On the other hand, the anomalous variation of the mobility at lower temperatures does not follow impurity scattering. We argue that the observed behavior can perhaps be explained by a resonant scattering of electrons by defects. It has been shown that substitutional impurities with a large central-cell potential can give rise to levels above the conduction-band edge in semiconductors [38]. Such levels are narrow resonances because there is mixing with the conduction-band states. An electron at the energy of a resonance suffers strong scattering that can dominate other scattering mechanisms if the resonant level lies close enough to the conduction-band minimum [39]. It seems therefore plausible that the drop in mobility observed in lightly doped crystals is brought by the central-cell potential of resonant defects. As the localized levels of the defects move up in the conduction band with an increasing self-doping level, the central-cell scattering cross section becomes smaller, and other mechanisms start to dominate. For this reason, we do not observe a resonant effect in heavily doped crystals. It is worth mentioning that muon spin relaxation experiments show a significant change in the electronic states of CaB_6 and BaB_6 below $\approx$130 K, much like the resonant scattering effect observed in alkaline-earth-metal hexaborides [40].

The inset in Fig. 7 shows the variation of the Hall mobility in E_AB_6 single crystals with pressure. We observe that μ_H

increases with increasing pressure for the SrB_6-1 single crystal at 2 K. The carrier concentration for this sample does not change with pressure. On the other hand, μ_H slowly decreases upon applying pressure in the BaB_6-1 crystal for which n_{el} increases with p. To interpret these results, we will consider the ionized impurity scattering since this mechanism limits electron mobility at low temperatures. Within the Born approximation for strongly degenerated materials, the mobility is proportional to [41] $\mu \propto \epsilon^2(n_{el}/N_I)[1/m^*(E_F)]^2[1/F(\lambda, E_F)]$, where $m^*(E_F)$ is the effective mass, evaluated at the Fermi surface, and $F(\lambda, E_F)$ is the scattering function. Other symbols are defined above. For the case when the applied pressure does not affect n_{el}, the pressure-induced changes in the dielectric constant would lead to the observed rise in the electron mobility [42]. On the other hand, the rise in the carrier density under pressure leads to the increase in E_F and of $m^*(E_F)$. As the scattering function also becomes larger, the mobility decreases with pressure. However, taking into account the variation of the n_{el}/N_I term in the expression for the mobility may reverse this trend. We expect that the number of charged defects N_I does not change significantly with pressure since in our crystals the rate for the two-electron capture by the d^+ center and subsequent formation of d^- states is higher than the rate for capture of electrons by d^+ states and subsequent formation of neutral states d^0. Therefore, the variation of the n_{el}/N_I counterbalances the decrease in mobility brought by the band effects and starts to dominate for high pressures. The $\mu_H(p)$ behavior at 80 K for the BaB_6-1 crystal, shown in Fig. 7, is consistent with these predictions.

C. Magnetoresistance

The single crystals we study are self-doped intrinsic semiconductors. When the defect concentration is large enough, there is an insulator-metal (MI) transition arising from shallow impurity-state overlap. A sharp drop in low-temperature Hall mobility at $n_{el} \approx 1 \times 10^{18}$ cm^{-3}, which we reported for CaB_6 crystals [20], corresponds to the MI transition in this system. The product $k_F l$, where $l = (\hbar/e)k_F\mu$ is the mean-free path, is frequently used to assess the conduction regime of the material. We find that, for lightly doped samples, $k_F l$ is much smaller than 1, which suggests a strongly localized regime. Most of our crystals however are either in the critical region ($k_F l \simeq 1$) or on the metallic side of the MI transition in a weakly localized regime (WLR) for which $k_F l > 1$.

Our discussion of the MR in E_AB_6 single crystals is mainly based on localization and Coulomb interaction models for disordered systems [43]. The localization term lowers conductivity as temperature decreases. On the other hand, Coulomb interactions give a temperature correction to $\sigma(0)$ of the form $\sqrt{T}$ that can change sign as the screening length varies [44]. In particular, electron-electron scattering at low temperatures leads to $\sigma(T) = \sigma(0)[1 + fA(T/T_o)^{1/2}]$ [45]. Here, $A = 0.72$, T_o is a characteristic temperature $T_o = T_F(k_F l)^3$, and $f = 1 - (3/2x)\ln(1+x)$, where $x = 2k_F/k_{TF}$ [46]. For the crystals we have studied, x varies between 1 and 2, which renders f positive, in agreement with the data plotted in Fig. 2. Therefore, the low-temperature variation of the conductivity in our samples most likely arises from Coulomb interactions.

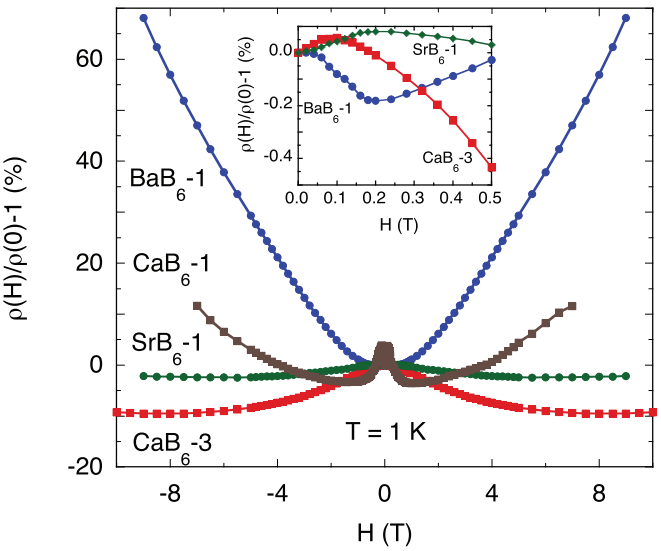

FIG. 8. Low-temperature magnetoresistance for E_AB_6 single crystals in different localization regimes. The low-field region is shown in the inset.

As mentioned above, multiple scattering (localization) can give rise to a drop in the conductivity for metallic samples [47]. Since the magnetic-field H suppresses localization, negative MR is often observed at high magnetic fields [48]. On the other hand, spin-orbit scattering can lead to negative corrections to $\sigma(T)$ through destructive-interference effects [49] and, therefore, to positive MR [43]. This effect should, in principle, be observed for compounds with high atomic numbers [50]. Furthermore, Zeeman splitting can also be important for positive MR in metallic samples under certain conditions [51].

Our MR measurements on E_AB_6 single crystals show both positive and negative components. This is displayed in Fig. 8. Let us first discuss the negative MR which we observe for crystals in the WLR. When H is not very strong, the magnetic length is $l_h \equiv (c\hbar/eH)^{1/2} \gg l$, and at low temperatures, the leading term in magnetoconductivity $\Delta\sigma = \sigma(H) - \sigma(0)$ comes from the localization effect. It has a simple form: $\Delta\sigma(H,0) = 2.90\sqrt{H}$, where $\Delta\sigma$ is in units of Ω^{-1} cm^{-1} for H given in teslas [52]. For weak magnetic fields, $\Delta\sigma \propto H^2$. The data plotted in Fig. 9 seem to follow these predictions. We find that $\Delta\sigma \approx 3.5\sqrt{H}$ at intermediate fields. This is larger than the theoretical value of 2.9. The difference most likely comes from the anisotropy of the Fermi surface in CaB_6 [52]. Enhanced electron interactions in the presence of orbital and spin splitting effects in WLR lead to a positive MR [49,53]. This is observed at weak magnetic fields as shown for SrB_6-1 and CaB_6-3 crystals in the inset of Fig. 8. Generally, electron interaction corrections are much smaller than the negative localization effect.

The crystals in the critical or strongly localized regime show a positive MR as displayed in the inset of Fig. 9 for two samples. We find a quadratic dependence of the MR on the applied magnetic field as in the classical description of the Hall effect. However, the classical effect is usually rather small and is often masked by other contributions to the MR. Hopping conduction in the impurity band gives rise to an exponential

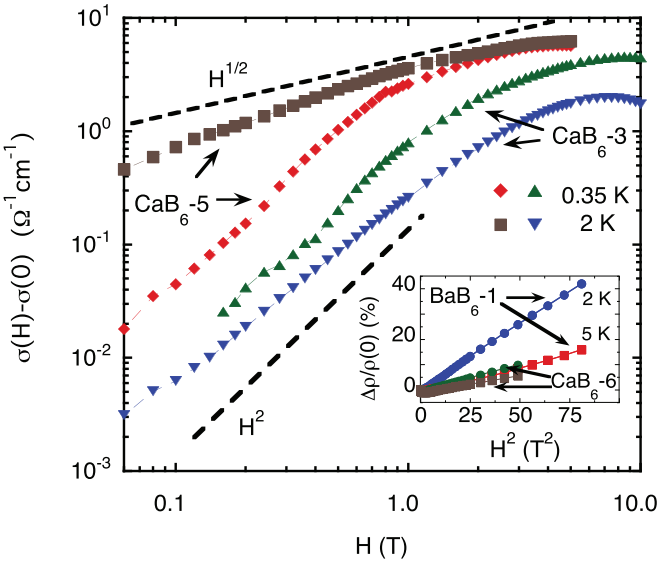

FIG. 9. Low-temperature magnetoconductance for CaB_6 single crystals in the weakly localized regime. The inset shows magnetoresistance as a function of the square of the magnetic field for the crystals in strongly localized and critical regimes.

dependence of the resistivity on temperature and magnetic field which comes from diamagnetic shrinking of the wave function [54,55]. We do not observe such behavior in our samples. We believe that the paramagnetic splitting of the conduction band and of the d^0 defect level is a likely explanation [51]. At the highest applied fields (near 10 T), this splitting is less than 1 meV for free electrons. Therefore, the Zeeman effect raises the density of states at the Fermi level only marginally for one spin band and lowers it for the other. Even so, its effect on the electron concentrations at low temperatures accounts for 0.2% in samples with $\approx 10^{19}$ defects per cm^{-3} and gives higher values for lightly doped crystals. Furthermore, including the splitting of the d^0 level leads to larger variations of n_{el} with the magnetic field. Consequently, the modeling of the MR behavior becomes quite complicated because of the various contributions and parameters it involves.

IV. CONCLUSIONS

To summarize, we have consistently explained the variation of the electrical resistivity and the Hall effect with temperature and hydrostatic pressure in E_AB_6 single crystals. This is achieved with a variable-charge defect model. The defects are intrinsic to all the alkaline-earth-metal hexaborides we have studied. They give rise to a narrow band, resonant with the conduction band, which effectively pins the Fermi level at low temperatures. In addition, a negatively charged, localized level of the same defect exists at a higher-energy level. This situation leads to a weak temperature and pressure variation of the electron concentration and mobility in E_AB_6 systems.

The low-temperature variation of the conductivity in these systems most likely arises from Coulomb interactions. These interactions are also responsible for a small positive magnetoresistance which we observe at low magnetic fields for samples in a weakly localized regime. A negative MR, which shows up at higher magnetic fields in heavily doped crystals, follows from localization effects. Lightly doped samples exhibit a large positive magnetoresistance that is difficult to model because of the variety of contributions involved.

ACKNOWLEDGMENTS

We acknowledge support from Grant No. MAT2012-38213-C02-01 from the Ministerio de Economía y Competividad of Spain. Additional support from Diputación General de Aragón (DGA-CAMRADS) is also acknowledged. Work at Los Alamos was performed under the auspices of the U.S. Department of Energy, Office of Basic Energy Sciences, Division of Materials Science and Engineering. P.F.S.R. acknowledges a Director's Postdoctoral Fellowship through the LANL LDRD program. P.S. acknowledges the support by the U.S. Department of Energy (BES) under Grant No. DE-FG02-98ER45707. We used Servicio General de Apoyo a la Investigación (SAI) of Universidad de Zaragoza in our research.

[1] D. P. Young *et al.*, Nature (London) **397**, 412 (1999).
[2] H. R. Ott *et al.*, Physica B **281-282**, 423 (2000).
[3] D. M. Edwards and M. I. Katsnelson, J. Phys.: Condens. Matter **18**, 7209 (2006).
[4] K. Maiti, Europhys. Lett. **82**, 67006 (2008).
[5] M. Li, H. Wang, K. Snoussi, L. Li, W. Yang, and C. Gao, J. Appl. Phys. **108**, 103710 (2010).
[6] Y. Li, J. Yang, X. Cui, T. Hu, C. Liu, Y. Tian, H. Liu, Y. Han, and C. Gao, Phys. Status Solidi B **248**, 1162 (2011).
[7] A. N. Kolmogorov, S. Shah, E. R. Margine, A. K. Kleppe, and A. P. Jephcoat, Phys. Rev. Lett. **109**, 075501 (2012).
[8] G. Zhao, L. Zhang, L. Hu, H. Yu, G. Min, and H. Yu, J. Alloys Compd. **599**, 175 (2014).
[9] S. Massidda, A. Continenza, T. M. Pascale, and R. Monnier, Z. Phys. B **102**, 83 (1997); S. Massidda, R. Monnier, and E. Stoll, Eur. Phys. J. B **17**, 645 (2000).
[10] H. J. Tromp, P. van Gelderen, P. J. Kelly, G. Brocks, and P. A. Bobbert, Phys. Rev. Lett. **87**, 016401 (2001).
[11] B. Lee and L.-W. Wang, Appl. Phys. Lett. **87**, 262509 (2005).
[12] J. D. Denlinger, J. A. Clack, J. W. Allen, G.-H. Gweon, D. M. Poirier, C. G. Olson, J. L. Sarrao, A. D. Bianchi, and Z. Fisk, Phys. Rev. Lett. **89**, 157601 (2002).
[13] S. Souma, H. Komatsu, T. Takahashi, R. Kaji, T. Sasaki, Y. Yokoo, and J. Akimitsu, Phys. Rev. Lett. **90**, 027202 (2003).
[14] K. Giannó, A. V. Sologubenko, H. R. Ott, A. D. Bianchi, and Z. Fisk, J. Phys.: Condens. Matter **14**, 1035 (2002).
[15] Z. Fisk, H. R. Ott, V. Barzykina, and L. P. Gor'kov, Physica B **312-313**, 808 (2002).
[16] S. Paschen, D. Pushin, M. Schlatter, P. Vonlanthen, H. R. Ott, D. P. Young, and Z. Fisk, Phys. Rev. B **61**, 4174 (2000).
[17] P. Vonlanthen, E. Felder, L. Degiorgi, H. R. Ott, D. P. Young, A. D. Bianchi, and Z. Fisk, Phys. Rev. B **62**, 10076 (2000).

[18] H. R. Ott, M. Chernikov, E. Felder, L. Degiorgi, E. G. Moshopoulou, J. L. Sarrao, and Z. Fisk, Z. Phys. B **102**, 337 (1997).
[19] R. Monnier and B. Delley, Phys. Rev. Lett. **87**, 157204 (2001).
[20] J. Stankiewicz, J. Sesé, G. Balakrishnan, and Z. Fisk, Phys. Rev. B **90**, 155128 (2014).
[21] J. Friedel, Can. J. Phys. **34**, 1190 (1956).
[22] J. P. Heremans, B. Wiendlocha, and A. M. Chamoire, Energy Environ. Sci. **5**, 5510 (2012).
[23] ElectroLAB Company, Chiba, Japan.
[24] D. J. Chadi and K. J. Chang, Phys. Rev. B **39**, 10063 (1989).
[25] W. Shockley and J. T. Last, Phys. Rev. **107**, 392 (1957).
[26] D. C. Look, Phys. Rev. B **24**, 5852 (1981).
[27] S. K. Estreicher, M. Sanati, D. West, and F. Ruymgaart, Phys. Rev. B **70**, 125209 (2004).
[28] C. O. Rodriguez, R. Weht, and W. E. Pickett, Phys. Rev. Lett. **84**, 3903 (2000).
[29] K.-F. Berggren and B. E. Sernelius, Phys. Rev. B **24**, 1971 (1981).
[30] R. A. Abram, G. J. Rees, and B. L. H. Wilson, Adv. Phys. **27**, 799 (1978).
[31] T. Kurosawa, M. Matsui, and W. Sasaki, J. Phys. Soc. Jpn. **42**, 1622 (1977).
[32] T. Saso and T. Kasuya, J. Phys. Soc. Jpn. **48**, 1566 (1980).
[33] T. Suski, R. Piotrzkowski, P. Wisniewski, E. Litwin-Staszewska, and L. Dmowski, Phys. Rev. B **40**, 4012 (1989).
[34] G. Weill, I. A. Smirnov, and V. N. Gurin, J. Phys. (Paris) **41**, C5-185 (1980).
[35] R. Zallen and W. Paul, Phys. Rev. **155**, 703 (1967).
[36] X. Li, X. Huang, D. Duan, G. Wu, M. Liu, Q. Zhuang, S. Wei, Y. Huang, F. Li, Q. Zhou, B. Liu, and T. Cui, RSC Adv. **6**, 18077 (2016).
[37] P. M. Mooney, J. Appl. Phys. **67**, R1 (1990).
[38] H. P. Hjalmarson, P. Vogl, D. J. Wolford, and J. D. Dow, Phys. Rev. Lett. **44**, 810 (1980).
[39] O. F. Sankey, J. D. Dow, and K. Hess, Appl. Phys. Lett. **41**, 664 (1982).
[40] S. Kuroiwa, H. Takagiwa, M. Yamazawa, J. Akimitsu, A. Koda, R. Kadono, K. Ohishi, W. Higemoto, and I. Watanabe, Sci. Technol. Adv. Mater. **7**, 12 (2006).
[41] W. Zawadzki, in *Handbook of Semiconductors*, edited by W. Paul (North-Holland, Amsterdam, 1982), Vol. 1, p. 725.
[42] Z. Wasilewski and R. A. Stradling, Semicond. Sci. Technol. **1**, 264 (1986).
[43] P. A. Lee and T. V. Ramakrishnan, Rev. Mod. Phys. **57**, 287 (1985).
[44] T. F. Rosenbaum, K. Andres, G. A. Thomas, and P. A. Lee, Phys. Rev. Lett. **46**, 568 (1981).
[45] B. L. Altshuler and A. G. Aronov, Zh. Eksp. Teor. Fiz. **77**, 2028 (1979) [Sov. Phys. JETP **50**, 968 (1979)].
[46] B. L. Altshuler, A. G. Aronov, and P. A. Lee, Phys. Rev. Lett. **44**, 1288 (1980).
[47] G. Bergmann, Phys. Rep. **107**, 1 (1984).
[48] A. Kawabata, J. Phys. Soc. Jpn. **49**, 628 (1980).
[49] H. Fukuyama and K. Hoshino, J. Phys. Soc. Jpn. **50**, 2131 (1981).
[50] N. F. Mott, *Metal-Insulator Transitions* (Taylor & Francis, London, 1990).
[51] G. Xiong, S.-D. Wang, and X. R. Wang, Phys. Rev. B **61**, 14335 (2000).
[52] Y. Ootuka and A. Kawabata, Prog. Theor. Phys. Suppl. **84**, 249 (1985).
[53] B. L. Altshuler, and A. G. Aronov, in *Electron-Electron Interactions in Disordered Systems*, edited by M. Pollak and A. L. Efros (North-Holland, Amsterdam, 1985).
[54] B. I. Shklovskii and A. L. Efros, *Electronic Properties of Doped Semiconductors* (Springer-Verlag, New York, 1984).
[55] D. M. Finlayson, J. Irvine, and L. S. Peterkin, Philos. Mag. B **39**, 253 (1979).